REPORT SERIES IN AEROSOL SCIENCE
N:o 235 (2021)

Growth and Melting of Atmospheric Ice Particles: Insights from Radar Observations

Haoran Li

Institute for Atmospheric and Earth System Research / Physics
Faculty of Science
University of Helsinki
Helsinki, Finland

Academic dissertation

To be presented, with the permission of the Faculty of Science of the University of Helsinki, for public criticism in Chemicum auditorium A110, A. I. Virtasen aukio 1, on January 8th, 2021, at 14 o'clock.

Helsinki 2021

Author's Address: Institute for Atmospheric and Earth System Research / Physics
P.O. Box 64
FI-00014 University of Helsinki
haoran.li@helsinki.fi

Supervisor: Associate Professor Dmitri Moisseev, Ph.D.
Institute for Atmospheric and Earth System Research / Physics
University of Helsinki

Reviewers: Senior Research Scientist, Sergey Matrosov, Ph.D.
Physical Sciences Laboratory
NOAA

Professor Johannes Verlinde, Ph.D.
Department of Meteorology and Atmospheric Science
Pennsylvania State University

Opponent: Professor Steve Nesbitt, Ph.D.
Department of Atmospheric Sciences
University of Illinois at Urbana-Champaign

ISBN 978-952-7276-51-8 (printed version)
ISSN 0784-3496
Helsinki 2021
Unigrafia Oy

ISBN 978-952-7276-52-5 (pdf version)
http://www.FAAR.fi
Helsinki 2021

Acknowledgements

The research in this thesis was conducted at the Institute for Atmospheric and Earth System Research (INAR) / Physics, University of Helsinki and supported by China Scholarship Council. I appreciate the head of INAR Prof. Markku Kulmala for providing me with a nice working environment and excellent facilities. I thank Prof. Steve Nesbitt for agreeing to act as my official opponent. I also thank my thesis pre-examiners, Dr. Sergey Matrosov and Prof. Johannes Verlinde, for taking time to review this thesis. Marina Kurtén, MA, is acknowledged for improving the language of this thesis.

I would like to express my deepest gratitude to my supervisor Prof. Dmitri Moisseev for taking me into the radar meteorology lab, for his patience, motivation, and immense knowledge. I usually came up with some unfettered thoughts, which finally found their way thanks to his guidance. I enjoyed our discussions at many afternoons, covering many topics from general academia to my doctoral research. Some ideas formulated in those afternoon discussions finally resulted in scientific publications.

Most of my office time was spent together with Jussi Tiira, my best friend and excellent help desk. Without his expertise on Linux, Python, as well as LaTeX I could not get on my research so smoothly. I want to thank Dr. Anakaisa von Lerber for her thoughtful and professional suggestions on my study. Particularly, I feel grateful to Matti Leskinen for patiently guiding me with accessing and interpreting radar data. I also appreciate Dr. Jani Tyynelä for his help on particle scattering. In past years, I have enjoyed working with Marta, Lorenzo, Tanel, Brandon, Sybille and José.

I thank Prof. Pavlos Kollias and Prof. Herman Russchenberg for motivating my interest in Doppler spectra during the Hyytiälä winter school in 2017. Dr. Stefan Kneifel is acknowledged for offering me timely help when I was struggling with analysing Doppler spectra data. I also appreciate the cooperation with Dr. Alexei Korolev.

I have learnt a lot from the ceilometer project led by Vaisala Oy. I would like to thank Prof. Ewan O′Connor, Prof. Lili Wang, Raisa, Hannamari and Minttu for their support and encouragement.

I feel fortunate to have so many great memories in Helsinki. I am very grateful to HYS for offering me nice accommodation. I wish to express my gratitude to my colleagues in INAR. I also want to thank my friends in the badminton club and table game club

for organizing wonderful activities.

Finally, I would like to thank my parents for their endless support and selfless love.

Haoran Li

Haoran Li
University of Helsinki, 2021

Abstract

Majority of precipitation in mid- to high-latitudes originates from ice clouds. In these clouds, atmospheric ice particles grow through various microphysical processes and may precipitate to the surface in the form of snowfall or rainfall. A large fraction of these clouds contain supercooled liquid water, which affects microphysical properties of ice particles. However, despite the importance of ice microphysics in mixed-phase clouds to the development of precipitation, our understanding of underlying processes is still lacking.

In past decades, long-term continuous observations of clouds and precipitation have shown promise for addressing this challenge. To provide such observations, remote sensing instruments, such as weather and research cloud radars, have been widely utilized. In this thesis, operational weather radars and cloud radars are used to address some challenges specific to ice microphysics.

Using dual-polarization weather radar observations collected over four years, we show how the shape of ice particles depends on rime mass fraction and present the parametrization of this dependence. This study also investigates the potential of using radar dual-polarization signatures to identify riming extent. Furthermore, the complexity of ice microphysics and the ambiguity of corresponding radar signatures motivate search for additional information, which can be used to infer ice microphysics. This work illustrates how radar characteristics of the melting layer can be linked to ice growth processes such as riming and aggregation.

In natural clouds, ice particles are usually characterized by a large variety of habits. However, our interpretation of the melting layer usually assumes presence of a single class of ice particles with a certain shape. This study reports that two types of ice particles can produce different radar polarimetric signals in the melting layer. The melting signal of ice needles is employed to evaluate current melting layer detection methods.

The melting layer of precipitation also plays a negative role, because it attenuates radio waves. Due to this largely unknown attenuation at milimeter wavelengths, cloud properties in rainfall are poorly documented by ground-based cloud radars. In this study, the melting layer attenuation at Ka- and W-bands is quantified using the differential attenuation technique based on multifrequency radar Doppler spectra observations. In addtion, the retrievals are used to evaluate previous modelling results.

Keywords: Mixed-phase clouds, riming, melting layer, dual-polarization radar, multifreqency radar, radar Doppler spectra

Contents

List of publications

This thesis consists of an introductory review, followed by four research articles. In the introductory part, these papers are cited according to their roman numerals. **Papers I and IV** are reprinted under the agreement between Haoran Li (me) and John Wiley and Sons. **Paper II** is reprinted under Creative Commons Attribution 4.0 License. **Paper III** is reprinted under Creative Commons CC BY license.

I Li, H., Moisseev, D., & von Lerber, A. (2018). How does riming affect dual-polarization radar observations and snowflake shape?. Journal of Geophysical Research: Atmospheres, 123(11), 6070-6081.

II Li, H., Tiira, J., von Lerber, A., & Moisseev, D. (2020). Towards the connection between snow microphysics and melting layer: Insights from multi-frequency and dual-polarization radar observations during BAECC. Atmospheric Chemistry and Physics, 20, 9547-9562.

III Li, H., & Moisseev, D. (2020). Two layers of melting ice particles within a single radar bright band: Interpretation and implications. Geophysical Research Letters, 47, e2020GL087499.

IV Li, H., & Moisseev, D. (2019). Melting layer attenuation at Ka- and W-bands as derived from multifrequency radar Doppler spectra observations. Journal of Geophysical Research: Atmospheres, 124(16), 9520-9533.

1 Introduction

In mid- to high-latitudes, the majority of precipitation originates from ice (Mülmenstädt et al., 2015; Field and Heymsfield, 2015). Ice particles grow from small crystals to large snowflakes through a number of microphysical processes. Different processes have distinct impacts on physical properties of ice particles, leading to changes of surface precipitation intensity and accumulation (Mitchell et al., 1990; Houze Jr and Medina, 2005; Moisseev et al., 2017). As the ambient temperature of falling ice particles exceeds the melting point, they melt into raindrops. The ice melting process can modify the thermal structure of the melting layer (Stewart et al., 1984; Carlin and Ryzhkov, 2019) and may change the dynamics of precipitation (Heymsfield, 1979; Szeto et al., 1988).

Ice crystals are usually generated via primary ice nucleation (homogeneous/ heterogeneou nucleation) at a cloud top, and their number concentration may be amplified by secondary ice production (SIP) (Hallett and Mossop, 1974; Rangno and Hobbs, 2001). After ice particles are formed, they can grow through a number of pathways (Figure 2). Ice crystal habits are formed during the vapor deposition growth, where temperature and supersaturation define the particle shape. Besides, ice crystals may collide and stick together, resulting in larger aggregates. In presence of supercooled liquid droplets, vapor deposition growth can be enhanced at expense of supercooled liquid water through Wegener-Bergeron-Findeisen (WBF) process (Korolev, 2007). Ice particles can also directly accrete supercooled liquid water through riming, which contributes to the ice mass growth. When they descend below the 0 °C isothermal layer, the ice melting process starts. These microphysical processes have been parameterized in numerical models and are important for the development of precipitation (Thompson et al., 2004; Gilmore et al., 2004). However, microphysics schemes are facing major challenges and one of them roots from our knowledge gap of the underlying microphysical processes such as the growth and melting of ice particles (Morrison et al., 2020).

Field observations have the potential to bridge this gap (Korolev et al., 2017; Field et al., 2017; Morrison et al., 2020). In situ instruments directly observe microphysical properties of ice particles, and can be deployed on aircrafts. However, aircraft measurements are limited by their relatively small sampling volumes and are only available from campaigns. Observations of clouds and precipitation may also be obtained by ground-based radars. Thanks to their high temporal and spatial resolutions, long-term

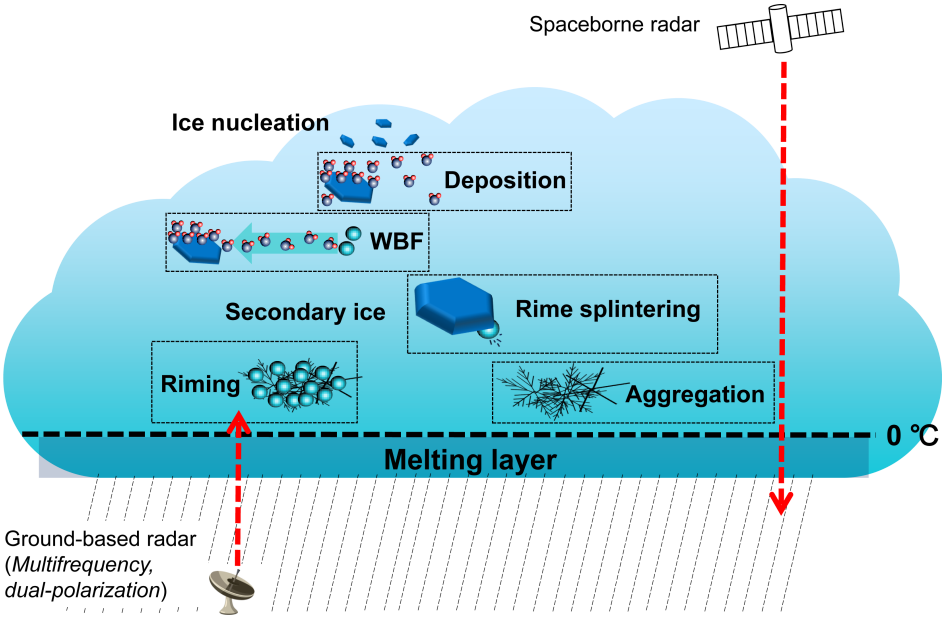

Figure 1: Overview of mixed-phase cloud processes and radar observations.

continuous radar observations may be used to elucidate ice microphysical processes. Recent studies have leveraged observations from dual-polarization and multifrequency (e.g., X-, Ka- and W-bands) radars to advance our understanding of ice microphysical processes in mixed-phase clouds (e.g., Kneifel et al., 2015, 2016; Vogel and Fabry, 2018; Oue et al., 2018; Mason et al., 2018, 2019).

Dual-polarization radar observations are sensitive to the microphysical properties of ice particles (Giangrande et al., 2016; Kumjian et al., 2016; Moisseev et al., 2017). For example, the ice growth during riming is expected to increase the aspect ratio of ice particles (Heymsfield, 1982; Garrett et al., 2015) and change radar polarimetric signatures (Straka et al., 2000; Giangrande et al., 2016; Vogel and Fabry, 2018). This riming impact on ice shapes is important for predicting the ice mass growth and has been parameterized in recent ice microphysics schemes (Morrison and Grabowski, 2008; Morrison and Milbrandt, 2015). This parameterization of ice crystals has been evaluated by wind tunnel experiments (Jensen et al., 2017). However, there is a lack of observations which can be used to quantify the riming impact on snow aggregates. In **Paper I**, we investigate the riming impact on the shape of aggregated snowflakes based on the combination of surface instrument and dual-polarization weather radar observations.

Although different ice growth processes have various impacts on ice microphysics, their radar manifestations are usually ambiguous. In **Paper I**, we show that rimed snowflakes and aggregated snowflakes have similar radar polarimetric signatures. Alternatively, previous studies (e.g., Zawadzki et al., 2005; Kumjian et al., 2016; Carlin and Ryzhkov, 2019) have suggested that ice growth processes can be inferred from the melting signatures of ice particles. However, the consensus on the interpretation of melting signatures is yet to be reached (e.g., Kumjian et al., 2016; Carlin and Ryzhkov, 2019). Furthermore, because previous studies have mainly focused on case analysis (e.g., Zawadzki et al., 2005; Kumjian et al., 2016; Xie et al., 2016; Carlin and Ryzhkov, 2019), there is a lack of comprehensive observations to link ice growth processes and the melting layer. In **Paper II**, we develop an algorithm to identify rimed and unrimed snowflakes, and investigate the link between ice growth precesses and the melting layer.

The melting layer in radar observations is usually manifested as a region of enhanced reflectivity factor, the so-called bright band (Fabry and Zawadzki, 1995). Our interpretation of this bright band and its polarimetric signatures is usually based on the assumption of a single population of ice particles with a certain shape (e.g., Russchenberg and Ligthart, 1996; Zawadzki et al., 2005; Fabry and Szyrmer, 1999; Kumjian et al., 2016). In practice, a number of studies have reported coexistence of multiple populations of ice particles in clouds (e.g., Zawadzki et al., 2001; Spek et al., 2008; Verlinde et al., 2013; Moisseev et al., 2015). This is important not only for investigating processes that take place in the melting layer, but also for understanding ice generation mechanisms, for example the SIP. In **Paper III**, we report how ice needles, potentially generated by the rime splintering process (Hallett and Mossop, 1974), and background ice particles affect radar observations of the melting layer and discuss its implications.

The melting of ice particles also negatively impacts radar retrievals of cloud properties, because it attenuates radar signals. Although, the melting layer attenuation is negligible for centimeter wavelength radars in cases where the propagation path through the melting layer is not too long (von Lerber et al., 2014), it can be significant at Ka- and W-bands (Matrosov, 2008). This affects ground- (e.g., Illingworth et al., 2007) and space-based (e.g., Mitrescu et al., 2010) radar retrievals of clouds and precipitation, respectively. Despite that some models have estimated the melting layer attenuation at Ka- and W-bands (Haynes et al., 2009; Matrosov, 2008), these model estimates need

to be validated by observations. In **Paper IV**, the melting layer attenuation at Ka- and W-bands is derived using the differential attenuation technique based on the multifrequency radar Doppler spectra observations, and compared with previous modelling estimates.

To summarize, this thesis aims to provide new insights into the ice growth and melting processes with the use of dual-polarization and multifrequency radar observations. The objectives of this thesis are,

1. Quantify the impact of riming on the snowflake shape and dual-polarization radar variables (**Paper I**)

2. Advance our understanding on the connection between ice growth and melting processes using multifrequency and dual-polarization radar observations (**Paper II**)

3. Identify the melting signatures of a mixture of needles and background ice, and evaluate different meltingl layer detection methods (**Paper III**)

4. Quantify the melting layer attenuation at Ka- and W-bands (**Paper IV**)

2 Precipitation formation in mixed-phase clouds

2.1 Ice initiation and depositional growth

Ice particles at the cloud top are formed by either homogeneous or heterogeneous nucleation. The homogeneous freezing of liquid water requires temperatures below -38°C. At higher temperatures, heterogeneous nucleation, which is facilitated by ice nucleating particles (INPs), is the dominant mechanism.

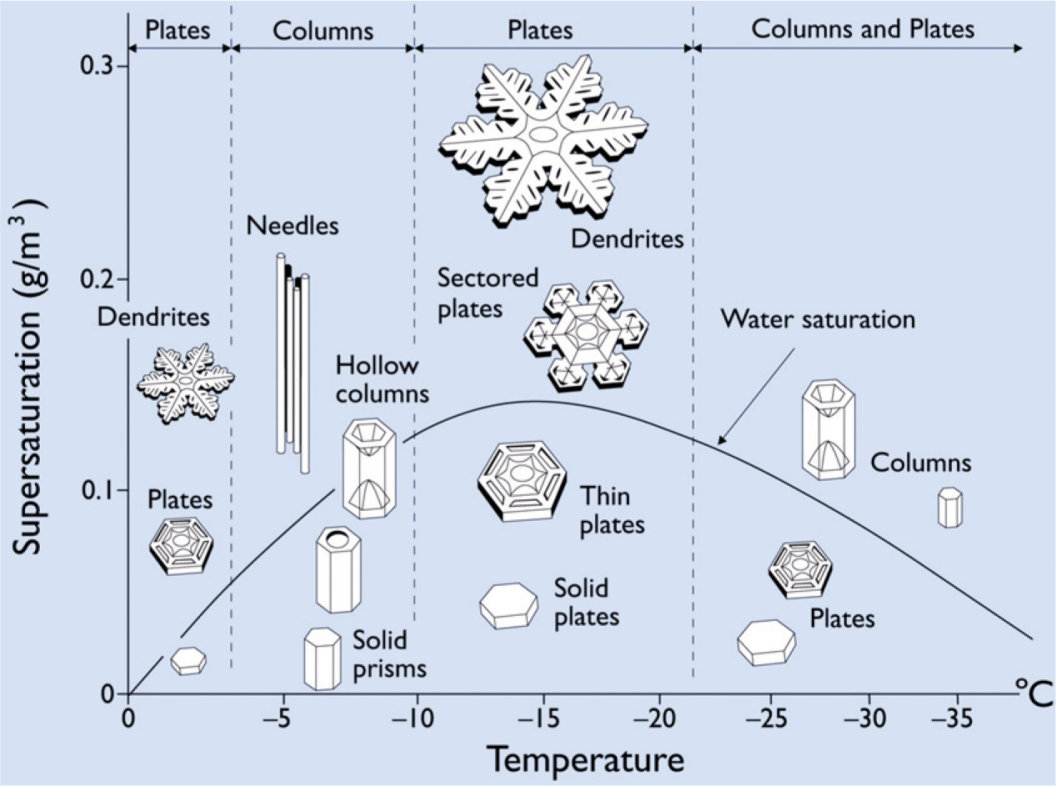

Figure 2: Morphology of ice crystals as a function of temperature and vapor supersaturation relative to ice. Adopted from (Libbrecht, 2005)

After nucleation, ice crystals grow by vapor deposition. The depositional growth leads to mass accumulation and habit formation. As shown in Figure 2, the basic habit of pristine ice crystals is mostly hexagonal. The primary ice habit (columnar/ platelike ice) is driven by temperature, because the ratio between the growth rates of the basal and prism faces is dependent on the temperature. For a given temperature, the detailed growth features of snowflakes can be different depending on the ice supersaturation.

At around -15 °C, ice dendrites are expected to form if the ice supersaturation is relatively high while at around -5 °C the formation of columnar ice particles is preferred. Since the ice supersaturation is relatively high in mixed-phase clouds, columnar ice particles formed within the temperature range of -8 $\sim$ -3 °C are expected to be needles. Therefore, they are referred to as ice needles in this thesis.

2.2 Secondary ice production

As the temperature increases, the expected number concentration of INPs generally decreases (e.g., Fletcher et al., 2011). At temperatures between -10 °C and 0 °C, the observed ice number concentration in clouds may be orders of magnitude higher than the expected number concentration of INPs (e.g., Mossop, 1985; Hobbs and Rangno, 1985; Rangno and Hobbs, 2001). Therefore, it has been suggested that secondary ice production (SIP) processes may exist to amplify the concentration of primary ice particles generated by homogeneous or heterogeneous nucleation (Field et al., 2017). It is currently hypothesized that the SIP may occur in clouds via rime splintering (Hallett and Mossop, 1974), droplet shattering on freezing (Johnson and Hallett, 1968), mechanical fragmentation upon collisions of ice crystals (Vardiman, 1978), and sublimation fragmentation (Oraltay and Hallett, 1989), as schematically depicted in Figure 3.

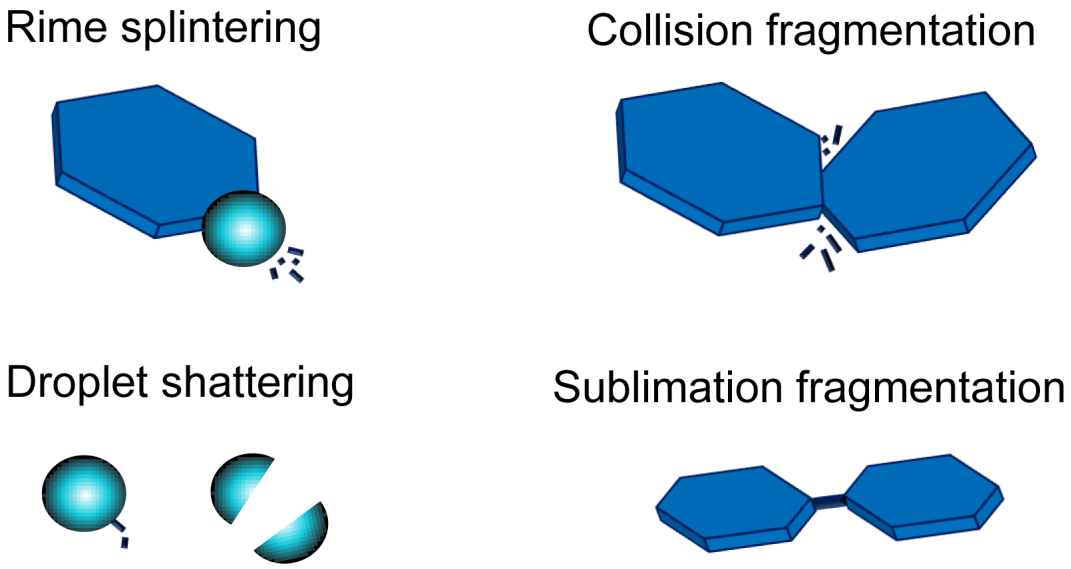

Figure 3: Mechanisms of SIP as summarised in (Field et al., 2017)

In numerical models, such as the Weather Research and Forecasting model (Skamarock et al., 2008; Morrison et al., 2005), the rime splintering process is the only SIP mechanism that has been parameterized thanks to early quantitative laboratory experiments (Hallett and Mossop, 1974) and numerous observations of high ice particle concentrations in the corresponding temperature regime (e.g., Hallett et al., 1978; Hogan et al., 2002; Keppas et al., 2017). It was found that ice splinters can be generated upon the presence of liquid droplets with a diameter larger than 25 μm within the temperature range of $-8 \sim -3$ °C. In mixed-phase clouds, these ice splinters may grow to ice needles, which can be detected from radar polarimetric Doppler spectra observations (Oue et al., 2015). This method is employed in **Paper III** to identify the presence ice needles which are potentially generated by the rime splintering process, which leads to the finding of two layers of melting ice particles.

2.3 Aggregation

Ice particles can collide and stick to each other to form aggregates. These particles are larger than the original ice particles and tend to have higher fall velocities. As a result, this process leads to the increase of ice mass flux, and therefore is important for precipitation development. Observations show that the largest snowflakes are found at around -15 °C and 0 °C (Lamb and Verlinde, 2011), indicating aggregation is more active at those temperatures. At around -15 °C, the formation of dendrites is preferred. Their arms are usually protruding and they can easily hook each other. If the temperature is just several Celsius below 0 °C, strong ice aggregation may be explained by the sintering (Lamb and Verlinde, 2011).

2.4 Riming

In presence of supercooled liquid droplets, ice particles can collide and collect these liquid droplets, which is referred to as riming. Riming is an important ice mass growth process and may contribute to $40 \sim 100$ % surface snow mass accumulation (Harimaya and Sato, 1989; Mitchell et al., 1990; Moisseev et al., 2017). The ratio of accreted ice mass to the total snow mass is defined as rime mass fraction (FR) in numerical models (Morrison and Grabowski, 2008; Morrison and Milbrandt, 2015) and a recent observational study (Moisseev et al., 2017). Riming transforms the shape of ice particles,

and the parameterization of this process is important in some ice microphysics schemes (Morrison and Grabowski, 2008; Morrison and Milbrandt, 2015). It has been hypothesised that riming may be described as a two-stage growth process (Heymsfield, 1982). At the first stage, particle dimensions are preserved while riming fills in the unoccupied space and the mass of ice particles increases. Then, the aspect ratio increases until the formation of graupel. For single ice crystals, Jensen et al. (2017) have quantified the impact of riming on ice habits and compared the results with wind tunnel observations. However, for snow aggregates, there is still a lack of observations which can be used to validate this hypothesis. In **Paper I**, the riming impact on the shape of snowflakes is investigated based on the combination of surface in situ and dual-polarization radar observations.

2.5 Melting

The melting layer is the region where the transition from snowflakes to raindrops takes place. Although the thickness of the melting layer is usually just several hundred meters, the latent cooling released during the phase transition can modify the dynamics of precipitation (Heymsfield, 1979; Szeto et al., 1988) and change the surface precipitation type (Kain et al., 2000). The microphysical processes taking place in the melting layer are rather complex and there is an ongoing debate on which processes should be included in melting layer models and which ones can be omitted. For example, the early study by Ohtake (1969) indicates that the melting process does not change the particle size distribution, and Barthazy et al. (1998) suggests that one snowflake melts into one raindrop. In contrast, Yokoyama et al. (1985); Heymsfield et al. (2015) have found that the aggregation of ice particles still proceeds after the melting process starts. The complexity of the breakup of ice particles in the melting layer has been revealed in a recent modelling study (Leinonen and von Lerber, 2018), which shows that low-density snow aggregates tend to break up during melting, while heavily rimed snowflakes are less prone to the breakup.

In radar observations, the melting layer is usually manifested as a region of enhanced radar reflectivity factor, so-called bright band (Fabry and Zawadzki, 1995). It has been shown that radar characteristics of the melting layer, such as the strength (Zawadzki et al., 2005) and the location (Kumjian et al., 2016; Carlin and Ryzhkov, 2019) of the bright band, may be linked to different ice growth processes. However, there is a lack

of statistical studies addressing this link and the cause of local sagging of the bright band (saggy bright band) is still on debate (Kumjian et al., 2016; Carlin and Ryzhkov, 2019). In **Paper II**, we revisit the link between ice growth processes and the melting layer based on statistics of radar observation obtained during the Biogenic Aerosols - Effects on Clouds and Climate (BAECC) experiment (Petäjä et al., 2016).

Our interpretation of the melting layer usually assumes presence of a single class of ice particles (e.g., Fabry et al., 1992; Russchenberg and Ligthart, 1996; Zawadzki et al., 2001; Carlin and Ryzhkov, 2019). In practice, the co-existence of multiple ice types in clouds has been reported in a number of studies (e.g., Zawadzki et al., 2001; Spek et al., 2008; Oue et al., 2015; Verlinde et al., 2013) and the corresponding ice melting process has not been studied. In addition, it is not clear whether and how their melting signatures can be used to infer ice microphysical processes taking place above. In **Paper III**, we present radar observations of the melting of multiple populations of ice and use the melting signal of ice needles to evaluate current melting layer detection methods.

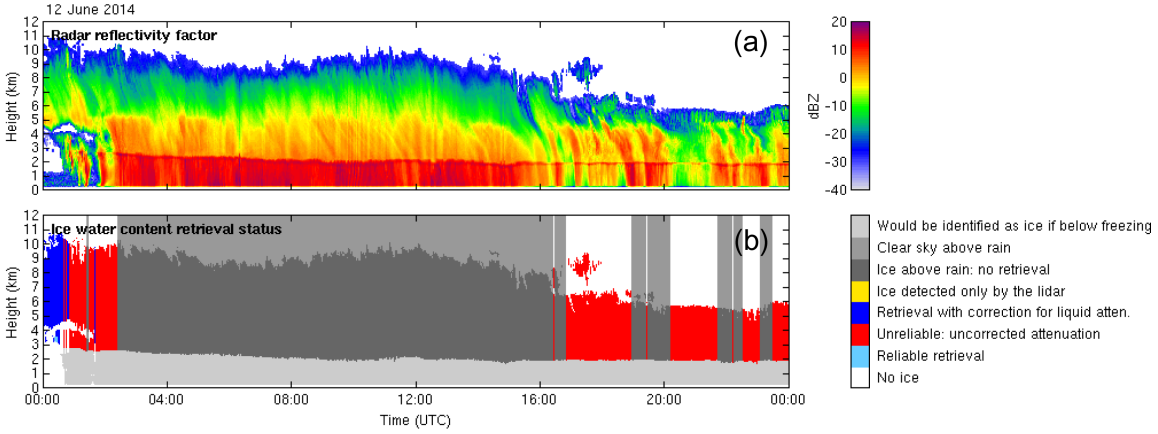

Figure 4: CloudNet radar data products from Hyytiälä. (a) Ka-band radar reflectivity factor and (b) ice water content retrieval status.

In addition, the melting of ice particles can strongly attenuate the microwave signals at milimeter wavelengths, hence biasing radar and passive microwave radiometer retrievals (Bauer et al., 1999; Battaglia et al., 2003; Matrosov, 2008; Haynes et al., 2009). For example, Figure 4 presents a stratiform rainfall event and the corresponding data products within the frame of CloudNet (Illingworth et al., 2007). The observed Ka-band radar reflectivity factor is shown in Figure 4 (a) and the melting layer is clearly identifiable at around 2 km. However, no retrievals above the melting layer can be

made (Figure 4 b) because of the unknown melting layer attenuation. Therefore, to advance our knowledge of cloud processes especially in precipitating systems based on cloud radars, the melting layer attenuation at milimeter wavelengths needs to be estimated. In **Paper IV**, the melting layer attenuation at Ka- and W-bands is derived based on the use of multifrequency radar Doppler spectra observations.

3 Basics of radar measurements

There are two approaches to observe ice microphysics in clouds and precipitation: in situ and remote sensing measurements. In situ instruments are usually deployed on aircrafts or the surface. Airborne sensors can directly measure properties of ice particles and liquid droplets in clouds, but their observations are constrained to narrow corridors of aircraft tracks and usually available from a limited number of campaigns. When ice/liquid particles descend to the surface, they can also be observed by ground-based optical distrometers such as 2-Dimensional Video Distrometer (Kruger and Krajewski, 2002), Multi-Angle Snowflake Camera (Garrett et al., 2012) and Particle Imaging Package (Newman et al., 2009; Tiira et al., 2016). These ground-based in situ measurements allow the direct analyse of image projections of hydrometeors (Garrett et al., 2015) and the retrieval of ice microphysics (Tiira et al., 2016; von Lerber et al., 2017). In spite of the unique capabilities of in situ observations in studying ice microphysics, they are not able to provide continuous observations of the vertical evolution of precipitation.

Atmospheric radars, alone or in combination with other remote sensing measurements, are utilized to fill this gap (e.g., Illingworth et al., 2007). They are active remote sensing instruments and can be installed on various platforms. Radars carried by satellites have the advantage of global coverage, but they are limited by relatively low temporal and spatial resolutions. Ground-based radars can provide long term observations of local clouds and precipitation with high temporal and spatial resolutions. The dual-polarization upgrade of atmospheric radars allows the retrieval of more detailed physical properties of hydrometeors. Recently, the development of multifrequency (e.g., X-, Ka- and W-bands) radar setup has also shown promise for inferring ice microphysics (e.g., Kneifel et al., 2015; Leinonen et al., 2018; Mason et al., 2019).

3.1 Radar equations

The meteorological applications of radars were recognized in World War II when weather echoes sometimes caused false alarms (Rauber and Nesbitt, 2018). Since then, radars have been utilized in observing meteorological targets.

The interpretation of radar measurements is based on the radar equation:

$$P_r = \frac{P_t G_t}{4\pi R^2} \frac{\sigma}{4\pi R^2} \frac{G_r \lambda^2}{4\pi} \frac{1}{L} \tag{1}$$

where P_r and P_t are the received and transmitted power, respectively, G_t and G_r are the antenna gains in transmitter and receiver, respectively. L is the signal attenuation during propagation, and σ is the radar cross section of the single target. The term $\frac{G_r \lambda^2}{4\pi}$ describes the effective aperture of the receiving antenna. $\frac{1}{4\pi R^2}$ is a function of range R and accounts for the isotropic propagation of the radar signal.

In practice, the objects (e.g., raindrops, snowflakes, and hails) are distributed throughout a radar measurement volume. The sum of radar cross sections from all contributing hydrometeors is $\sum_{i=1}^{n} \sigma_i$. Therefore, the radar equation for a distributed target can be written as

$$\overline{P_r} = \frac{P_t G_t G_r \lambda^2}{64\pi^3} \frac{1}{R^4} \frac{1}{L} \sum_{i=1}^{n} \sigma_i. \tag{2}$$

Since the main lobe of the radar beam is usually assumed to be in the Gaussian shape, $2 \ln 2$ should be inserted in the denominator of Eq. 2:

$$\overline{P_r} = \underbrace{\frac{P_t G_t G_r \lambda^2}{64(2\ln 2)\pi^3}}_{\text{Hardware}} \underbrace{\frac{1}{R^4}}_{\text{Range}} \underbrace{\frac{1}{L}}_{\text{Attenuation}} \underbrace{\sum_{i=1}^{n} \sigma_i}_{\text{Targets}} . \tag{3}$$

As shown in Eq. 3, the received radar power depends on the radar hardware, range, propagation attenuation and backscattering properties of targets. Weather radars usually operate at centimeter wavelengths (e.g., S-band is used in America while C-band is widely implemented in Europe), where the propagation attenuation in rain and snow is mostly negligible. In contrast, the atmospheric attenuation should be considered for cloud radars.

Here, radar reflectivity, which is related to the radar cross section of a distributed target, is defined as

$$\eta = \frac{\sum_{i=1}^{n} \sigma_i}{V_c} \tag{4}$$

where V_{c} is the radar volume containing all targets, which scatter radar signals back to the radar receiver, and can be expressed as

$$V_{\mathrm{c}} = \frac{\pi c \tau \Phi^2 R^2}{8} \tag{5}$$

where c is the light speed, τ is the pulse length, and Φ is the radar beamwidth, respectively. Substituting Eq. 4 and Eq. 5 into Eq. 3, we obtain

$$\overline{P_r} = \frac{P_t G_t G_r \lambda^2 \tau \Phi^2}{1024(\ln 2)\pi^3} \frac{1}{R^2} \frac{1}{L} \eta. \tag{6}$$

According to the Rayleigh approximation, the backscattering cross section of a spherical particle can be expressed as (Bohren and Huffman, 2008)

$$\sigma_{Rayleigh} = \frac{\pi^5}{\lambda^4} |K|^2 D_{\mathrm{sph}}^6 \tag{7}$$

where D_{sph} is the diameter of the spherical particle, K is the dielectric factor:

$$K = \frac{\epsilon_{\mathrm{r}} - 1}{\epsilon_{\mathrm{r}} + 2} \tag{8}$$

where ϵ_{r} is the relative dielectric constant. Assuming all particles in a radar measurement volume have particle dimensions much smaller than the radar wavelengths), Eq. 4 can be expressed as

$$\eta = \frac{\sum_{i=1}^{n} \sigma_i}{V_{\mathrm{c}}} = \frac{\pi^5}{\lambda^4} |K|^2 \frac{\sum_{i=1}^{n} D_{\mathrm{sph,\,i}}^6}{V_{\mathrm{c}}} \tag{9}$$

Then, the radar reflectivity factor, the most widely used quantity in radar meteorology, is defined as:

$$Z = \frac{\sum_{i=1}^{n} D_{\mathrm{sph,\,i}}^6}{V_{\mathrm{c}}} = \frac{\lambda^4}{\pi^5 |K|^2} \eta \tag{10}$$

The unit of Z is $\mathrm{mm}^6\ \mathrm{m}^{-3}$, while it is usually expressed in dB scale:

$$\mathrm{dBZ} = 10 \log_{10}(Z) \tag{11}$$

3.2 Dual-polarization radar variables

In meteorological applications, hydrometeors are usually non-spherical and their backscattering properties depend on the polarization state of the incident electromagnetic wave. To use this dependence, modern radars employ dual-polarization technology, where the polarization states of the transmitter and receiver are controlled. Typically, horizontal and vertical linear polarizations are used.

In this case, the electric field of an electromagnetic wave can be written as

$$\overrightarrow{E_{\mathrm{I}}}(t) = |A_{\mathrm{I,H}}|\cos(\omega t + \phi_{\mathrm{H}})\,\overrightarrow{h} + |A_{\mathrm{I,V}}|\cos(\omega t + \phi_{\mathrm{V}})\,\overrightarrow{v} \tag{12}$$

where ω is the angular frequency, and $|A_{\mathrm{I,H}}|$ and $|A_{\mathrm{I,V}}|$ are amplitudes of horizontal (H) and vertical (V) polarizations components, ϕ_{H} and ϕ_{V} are phases of H and V components, and $\overrightarrow{h}$ and $\overrightarrow{v}$ are unit vectors that define the horizontal and vertical linear polarizations, respectively. The corresponding backscattering wave after the interaction with a particle can be described as

$$\overrightarrow{E_{\mathrm{S}}}(t) = \mathbf{S}\overrightarrow{E_{\mathrm{I}}}(t) \tag{13}$$

where $\mathbf{S}$ is the complex amplitude scattering matrix and is expressed as (Bringi and Chandrasekar, 2001)

$$\mathbf{S} = \frac{e^{-jkr}}{r}\begin{pmatrix} S^{\mathrm{hh}} & S^{\mathrm{hv}} \\ S^{\mathrm{vh}} & S^{\mathrm{vv}} \end{pmatrix} \tag{14}$$

where j is the square root of -1, k is the wavenumber, r is the distance between the particle and the observation point in the far field, respectively. Because of the reciprocity at backscattering, $|S^{\mathrm{vh}}|^2 = |S^{\mathrm{hv}}|^2$ (Bringi and Chandrasekar, 2001).

For a given radar frequency, the backscattering properties of a particle at horizontal and vertical polarizations are quantitatively characterized by $\mathbf{S}$. The backscattering cross sections for different transmitted/ received polarizations from a single particle are

$$\begin{aligned} \sigma_{\mathrm{hh}} &= 4\pi|S^{\mathrm{hh}}|^2, \\ \sigma_{\mathrm{vv}} &= 4\pi|S^{\mathrm{vv}}|^2, \\ \sigma_{\mathrm{hv}} &= 4\pi|S^{\mathrm{hv}}|^2. \end{aligned} \tag{15}$$

For a non-spherical particle, the radar reflectivity at horizontal polarization can be expressed as

$$\eta_{\mathrm{hh}} = \left\langle n4\pi |S^{\mathrm{hh}}|^2 \right\rangle \tag{16}$$

where n [m^{-3}] denotes the number density of particles in the radar volume and brackets $\langle\rangle$ denote averaging, respectively. Based on the definition of Z in Eq. 10, the horizontally polarized reflectivity factor is

$$Z_{\mathrm{hh}} = \frac{\lambda^4}{\pi^5 |K|^2} \left\langle n4\pi |S^{\mathrm{hh}}|^2 \right\rangle \ [\mathrm{mm}^6\ \mathrm{m}^{-3}]. \tag{17}$$

Similar to Eq. 17, the backscattered power at the vertical polarization Z_{vv} can also be derived.

3.2.1 Differential reflectivity

For a spherical particle, $S^{\mathrm{hh}} = S^{\mathrm{vv}}$, hence the backscattered radar power at two orthogonal polarizations are identical. The fact is that the shapes of meteorological targets in nature are usually not isotropic, and therefore the radar returns at two polarization channels are usually different. The difference between the backscattering radar powers at horizontal and vertical polarizations is described by differential reflectivity:

$$Z_{\mathrm{dr}} = 10 \log_{10} \frac{\left\langle n4\pi |S^{\mathrm{hh}}|^2 \right\rangle}{\left\langle n4\pi |S^{\mathrm{vv}}|^2 \right\rangle} = 10 \log_{10} \frac{Z_{\mathrm{hh}}}{Z_{\mathrm{vv}}} \ [\mathrm{dB}]. \tag{18}$$

Since hydrometeors have a preference for horizontal orientation, the radar return from the horizontal is often larger than the vertical. Thus, the Z_{dr} observed by weather radars is mostly non-negative when the elevation angle is close to 0°, despite that negative values may be observed for hail (Hubbert et al., 1998) and conical graupel (Bringi et al., 2017). Specifically, the observed Z_{dr} at the elevation angle of 0° is dependent on the density, phase, aspect ratio, canting angle and size distribution of hydrometeors present in the radar volume. For snowflakes, this dependence is simulated in **Paper I**. At the vertical incidence, the observed Z_{dr} is mostly close to 0 dB because the orientation angles of hydrometeors are usually uniformly distributed.

3.2.2 Linear depolarization ratio

In some cases, the polarization of the scattered wave is different from the incident. This effect in radar meteorology is known as depolarization. To quantify this effect, LDR is used:

$$\mathrm{LDR} = 10\log_{10}\frac{\left\langle n4\pi|S^{\mathrm{vh}}|^2\right\rangle}{\left\langle n4\pi|S^{\mathrm{hh}}|^2\right\rangle} = 10\log_{10}\frac{Z_{\mathrm{vh}}}{Z_{\mathrm{hh}}}\ [\mathrm{dB}] \tag{19}$$

where Z_{vh} is the backscattering power in the cross-polarization channel. Theoretically, the observed LDR depends on the intrinsic scattering properties of hydrometeors present in the radar volume (e.g., Tyynelä et al., 2011). In practice, the observed LDR is usually above -30 dB mainly due to the power leakage between polarization channels (Bringi and Chandrasekar, 2001; Moisseev et al., 2002).

Vertically pointing research radars often operate in the LDR mode, namely radar signals are transmitted from one polarization channel and received at orthogonal channels. In rain, the LDR signal of raindrops is usually lower than the noise level while it significantly increases in the melting layer. This allows the robust detection of the melting layer (Bringi and Chandrasekar, 2001). At the vertical incidence, ice particles with certain morphologies may produce distinctive LDR signals. Specifically, the W-band LDR of pristine columns and needles is around -15 dB (Aydin and Walsh, 1999; Oue et al., 2015), a level significantly higher than those of other ice types. This unique LDR feature facilitates the identification of needles from vertically pointing dual-polarization radar observations. In **Paper III**, LDR observations are used to analysis the presence of ice needles and characterize melting layer geometric properties.

3.2.3 Copolarized correlation coefficient

In statistics, the correlation coefficient is used to quantify the linear relationship between two variables. Similarly, the correlation between received signals at two polarization channels is defined as

$$\rho_{\mathrm{hv}} = \frac{\left|\left\langle S^{\mathrm{hh}}S^{\mathrm{vv}\ *}\right\rangle\right|}{\sqrt{\left\langle|S^{\mathrm{hh}}|^2\right\rangle\left\langle|S^{\mathrm{vv}\ *}|^2\right\rangle}}. \tag{20}$$

In radar applications, ρ_{hv} can be interpreted as a measure of the diversity of particle shapes, orientations, and phase states. This variable is useful regardless of radar an-

tenna elevation angle. The observed ρ_{hv} is close to 1 in rain and greater than $0.85 \sim 0.9$ in snow, while the magnitude of ρ_{hv} is generally from 0.7 to 0.95 in the melting layer (e.g., Bringi and Chandrasekar, 2001; Matrosov et al., 2007). The decrease of ρ_{hv} in the melting layer can be observed at any elevation angle and allows the identification the melting layer. In **Paper II** and **Paper IV**, ρ_{hv} is employed to determine the melting layer boundaries.

3.2.4 Specific differential phase

The speed of light depends on the refractive index of the medium. In clouds or precipitation, the refractive index of the medium is affected by the presence of hydrometeors. It turns out that horizontally polarized waves at low elevation angles are slower than vertically polarized ones, because hydrometeors are usually non-spherical and close to oblate shapes. This difference in the travelling time results in a relative phase shift between signals at H and V polarizations, which leads to differential phase shift Φ_{dp}. The range derivative of Φ_{dp} is known as specific differential phase:

$$K_{\mathrm{dp}} = \frac{1}{2}\frac{\mathrm{d}\Phi_{\mathrm{dp}}}{\mathrm{d}R} \quad [^{\circ}/\mathrm{km}] \tag{21}$$

where the term $\frac{1}{2}$ accounts for the phase shift occurring on the way to the radar volume and back. The observed K_{dp} depends on the concentration, shape, size and relative permittivity of nonspherical hydrometeors in a radar volume. At the vertical incidence, the observed K_{dp} is usually around $0\ ^{\circ}/\mathrm{km}$, because the orientation angles of hydrometeors are uniformly distributed and the phase shift between two polarizations is close to $0\ ^{\circ}$.

At horizontal incidence, which applies to most weather radar observations, the observed K_{dp} can be related to the rainfall intensity because larger raindrops are more oblate in shape and produce higher K_{dp} values. In snowfall, the observed K_{dp} depends on the concentration of non-spherical particles present along the radar beam. Therefore, the observed K_{dp} may be used to infer the microphysical properties of ice particles. In **Paper I**, the link between riming and K_{dp}-Z_{dr} is investigated.

3.3 Multifrequency radars

The backscattering properties of hydrometeors are usually different at various radar frequencies (e.g., Tyynelä et al., 2011). If the radar wavelength is relatively long and the Rayleigh scattering conditions are met, radar reflectivity factor is almost independent of the radar frequency (e.g., X-, C- and S-band radar observations of most hydrometeors). As the radar wavelength decreases towards the milimeter wavelength, the resonance scattering becomes more significant and the observed radar reflectivity factor may deviate from the value corresponding to the Rayleigh approximation. This phenomenon inspires the synergetic use of multifrequency radars to infer the characteristic size of hydrometeors which would be highly uncertain if a single radar frequency is employed. The dual-wavelength ratio (DWR) is defined as

$$DWR(\lambda_1, \lambda_2) = Z_{\lambda_1} - Z_{\lambda_2}, \ [\text{dB}] \tag{22}$$

where Z_{λ_1} and Z_{λ_2} are radar reflectivities at the wavelength of λ_1 and λ_2, respectively. As shown by Matrosov (1998), DWR(X,Ka) can be used to estimate the median volume diameter of snowflakes. In addition, more detailed information of ice particles may be inferred based on the combination of DWRs, e.g., DWR(X,Ka) and DWR(Ka,W) (Kneifel et al., 2015; Leinonen and Szyrmer, 2015). As shown by triple-frequency radar observations, rimed particles are usually characterized by small DWR(X,Ka) and high DWR(Ka,W), while the opposite has been observed for unrimed snow aggregates (Kneifel et al., 2015).

Currently, triple-frequency radar observations are limited to a few campaigns (e.g., Petäjä et al., 2016; Dias Neto et al., 2019), and the use of such observations is complicated by the attenuation. For example, the attenuation due to supercooled liquid water can be as large as 5 dB at W-band when the LWP is 500 g m^{-2} (Kneifel et al., 2015), and the resulting error in DWR(Ka,W) can significantly bias the retrieval of snow microphysics. Tyynelä and von Lerber (2019) have proposed the use of DWR(X,Ka) and Ka-band LDR to divide rimed and unrimed snowflakes by combining scattering models and field observations. However, the interpretation of LDR signals may be heavily affected by needle-type particles which can be generated by the rime splintering process (Oue et al., 2015) and co-exist with rimed snowflakes. Another approach to estimate the riming extent of snowflakes is the use of Doppler velocity measured by vertically

pointing radars. Mason et al. (2018) have compared different velocity-diameter relations and found that the fall velocity of snowflakes can be generally parameterized by the riming factor. In addition, the significant increase of DWR(X,Ka) seems to be related to the increase of the particle size during aggregation (Dias Neto et al., 2019). In **Paper II**, the potential of combining DWR(X,Ka) and X-band radar Doppler velocity in separating rimed and unrimed snowflakes is investigated.

3.4 Doppler spectra

Radar Doppler spectrum is the distribution of radar echoes over a range of sampled Doppler velocities. At the vertical incidence, the Doppler power spectrum in an idealized quiet environment can be expressed as

$$S_{\mathrm{hh},\ Q}(v) = \frac{\lambda^4}{\pi^5 |K|^2} N(D_{\max}) \sigma_{\mathrm{hh},b}(D_{\max}) \frac{\mathrm{d}D_{\max}}{\mathrm{d}v}\ [\mathrm{mm}^6\ \mathrm{m}^{-3}/\mathrm{m\ s}^{-1}] \tag{23}$$

where v and $\sigma_{\mathrm{hh},b}$ are particles' terminal velocity and backscattering cross section, respectively, as parameterized by the maximum diameter $D_{\max}$. Air motions, i.e., vertical air motions, turbulence and the cross wind, affect the observed Doppler power spectrum. This effect leads to the broadening of the Doppler spectrum and can be parameterized by convoluting a Gaussian function $g(v)$, which is characterized by a prescribed width σ_t, with $S_{\mathrm{hh},\ Q}$:

$$S_{\mathrm{hh},\ t} = S_{\mathrm{hh},\ Q} * g. \tag{24}$$

Considering the change of particles' fall velocities owing to vertical air motions, the observed Doppler power spectrum is

$$S_{\mathrm{hh},\ ob}(v) = S_{\mathrm{hh},\ t}(v + w_{\mathrm{air}}) \tag{25}$$

where w_{air} denotes the vertical air motion. Similarly, the spectral power at cross-polarization $S_{\mathrm{vh},\ ob}(v)$ can also be derived. By integrating the observed Doppler power spectrum, the radar reflectivity factor in Eq. 17 can be calculated as:

$$Z_{\mathrm{hh}} = \int_{-v_{\max}}^{v_{\max}} S_{\mathrm{hh},\ ob}(v) \mathrm{d}v \tag{26}$$

where $v_{\max}$ is the Nyquist velocity. Similarly, LDR can be expressed as:

$$\mathrm{LDR} = 10\log_{10}\frac{Z_{\mathrm{vh}}}{Z_{\mathrm{hh}}} = 10\log_{10}\frac{\int_{-v_{\max}}^{v_{\max}} S_{\mathrm{vh},\ ob}(v)\mathrm{d}v}{\int_{-v_{\max}}^{v_{\max}} S_{\mathrm{hh},\ ob}(v)\mathrm{d}v}. \tag{27}$$

If the broadening effect is negligible, i.e., $g(v)$ becomes the delta function, the observed radar Doppler spectrum can be approximated by Eq. 23. In this case, there will be a region in Doppler spectrum where the observed spectral powers at different radar bands are well matched. This region corresponds to the particles much smaller than all radar wavelengths, and usually resides at the slow-falling part of the Doppler spectrum.

Previous observational studies have shown that the regions where the Rayleigh scattering approximation applies in W-, Ka- and X-band radar Doppler spectra can be well matched in rain (Tridon et al., 2013) and in snow (Kneifel et al., 2016). Particularly, supercooled liquid droplets in mixed-phase clouds are usually rather small (Kollias et al., 2001), and are often manifested as an isolated spectral peak around 0 m/s in radar Doppler spectrum. Such spectral peaks facilitate the identification of particles satisfying the Rayleigh approximation in multifrequency radar Doppler spectra observations. In **Paper IV**, the regions where the Rayleigh scattering approximation is valid from multifrequency radar Doppler spectra observations are utilized to quantify the melting layer attenuation at Ka- and W-bands.

For vertically pointing dual-polarization radars operating in the LDR mode, the spectral LDR can be defined as

$$S_{\mathrm{LDR},\ ob}(v) = 10\log_{10}\frac{S_{\mathrm{vh},\ ob}(v)}{S_{\mathrm{hh},ob}(v)} \ \ [\mathrm{dB\ /\ m\ s^{-1}}]. \tag{28}$$

If the impact of spectral broadening can be neglected, $S_{\mathrm{LDR},\ ob}(v)$ depends only on the depolarization properties of targets. Therefore, $S_{\mathrm{LDR},\ ob}(v)$ can be used to separate columnar ice particles which usually produce LDR signals as high as -15 dB (Aydin and Walsh, 1999; Oue et al., 2015) in a radar volume. In **Paper III**, the polarimetric Doppler spectra observations are utilized to analyse the melting signatures of a mixture of needles and background ice.

4 Review of papers and the author's contribution

Paper I investigates the riming impact on snowflake shape and dual-polarization radar observations. The aspect ratio of snowflakes is derived by matching the T-matrix simulated and radar observed Z_{dr}. Results from four years of ground-based measurements confirm the two-stage evolution of snowflake aspect ratio during riming. At the first stage (FR < 0.5), the particle aspect ratio does not change much while the observed Z_{dr} increases due to the increase of particle density. After FR exceeds 0.5, the aspect ratio starts increasing, which leads to the rapid decrease of Z_{dr}. The results indicate that the aspect ratio of unrimed snowflakes is smaller than the widely-used value of 0.6. Furthermore, this study shows that the riming signatures seem to be diagnosable from the $Z_{\mathrm{dr}} - K_{\mathrm{dp}}$ space when Z > 15 dBZ.

The author's contribution: DM has conceived the study and took part in the data analysis. AvL has derived snowflake properties from ground-based observations that were used in this study. I have performed the majority of the data analysis, which included analysis and calibration of the C-band radar data, matching of ground-based and radar data, development and implementation of the retrieval algorithm. I also wrote the first draft of the manuscript, which was edited by all coauthors.

Paper II addresses the connection between snow microphysics and melting layer. A new method to classify unrimed and rimed snow from vertically pointing Ka- and X-band radars is derived. Ground-based observations and particle scattering databases are combined to simulate DWR(Ka,X) and Doppler velocity at X-band (V_{X}). The relations for classifying rimed and unrimed snow are derived and applied to vertically pointing Ka- and X-band radar observations during BAECC. The results show that precipitation intensity plays an important role in modulating the radar-observed melting layer properties and is highly associated with the sagging of bright band. Riming may contribute to the additional bright band sagging while the opposite is observed in light precipitation. Riming can also obscure the dip of radar reflectivity at the melting layer top. The enhanced aggregation close to the melting layer is evidenced by the observed decease of Z_{dr}. K_{dp} stays silent in light precipitation, and it starts to increase at around 3000 m above the melting layer top as the precipitation rate reaches 1 mm h $^{-1}$.

The author's contribution: DM and I have conceived the study. JT has derived vertical profiles of dual-polarization C-band radar observations over the measurement site,

which were used to make a connection between melting layer properties and dual-polarization signatures in ice clouds. I have performed the majority of the data preparation and analysis, which included data selection and handling, and multifrequency (X, Ka, W-band) radar data calibration, among other things. I have computed multi-frequency radar variables from ground-based observations of snowflake properties. The snowflake properties were computed by AvL. Based on these computations, I have designed the retrievals procedure that uses radar observations to estimate snowflake rime mass fraction. I have derived the statistics of the melting layer properties. Together with coauthors I have analyzed the results. I wrote the first draft of the manuscript, which was edited by all coauthors.

Paper III analyses the observed two layers of melting ice particles in a single radar bright band. This paper reports an interesting phenomenon of two layers of enhanced LDR within one layer of bright band. Such observations were recorded by vertically pointing W- and C-band radars. Doppler spectra observed by the W-band radar reveals that the first layer of enhanced LDR is attributed to the melting of newly-formed needles formed within the H-M temperature regime, while the second LDR layer is due to the melting of background ice. We found that the LDR of needles, very sensitive to the melting, can be used to evaluate the melting layer detection methods. The comparison shows that the bias of using Doppler velocity can be as large as 100 m, while the break point of C-band reflectivity is rather sensitive to the melting. In addition, we found that the observed LDR profile in the melting layer depends on the radar frequency. The identified melting layer bottom is lower for the C-band radar.

The author's contribution: Together with DM, we have conceived the study. I have identified the study cases and prepared the radar data. I have also performed most of the data analysis. I wrote the first draft, which was edited by DM.

Paper IV quantifies the melting layer attenuation at Ka- and W-bands. Multifrequency radar Doppler spectra observations are utilized to derive the melting layer attenuation at Ka- and W-bands. The rationale of this method is to use the differential attenuation between weak and strong attenuation radar bands. The region where the Rayleigh scattering approximation applies in the Doppler spectra is identified as the spectral region corresponding to slower falling particles, namely small ice crystals and liquid droplets. The derived attenuation at Ka- and W-bands overall agrees well with previous modelling studies but differences are found at high rain rates. Also, the results highlight that the W-band radar signal can be significantly attenuated by

supercooled liquid water.

The author's contribution: DM has conceived the study and took part in the analysis of the results. I have developed the attenuation estimation algorithm, designed and implemented software for reading and analyzing radar Doppler spectra data, and analyzed the results. I wrote the first draft of the paper, which was edited by DM.

5 Conclusions

The ice microphysical processes are crucial for the development of precipitation. The complex interactions between supercooled liquid and ice particles in mixed-phase clouds are still not well understood, leading to major uncertainties in numerical models (Morrison et al., 2020). This thesis studies the growth and melting processes of ice particles in stratiform precipitation based on the use of dual-polarization and multifrequency radar observations.

As an important ice growth process, riming not only substantially contributes to ice mass but also changes the particle shape. Using dual-polarization weather radar observations collected over four years, we show how the aspect ratio of snow aggregates changes with the increase of rime mass fraction and present the parameterization in **Paper I**. In addition, we analyse how dual-polarization radar observations (Z_{dr} and K_{dp}) are affected by riming, and find that it is challenging to unambiguously infer ice microphysics from radar observations. This ambiguity of radar signatures of the ice microphysics motivates the investigation of the link between ice microphysical processes and the radar characteristics of the melting layer. To investigate this link, an algorithm for separating unrimed and rimed snowflakes is developed and applied to radar observations recorded during BAECC in **Paper II**. Based on the statistics of radar observations, we show that the precipitation intensity is the dominating factor that influences the melting layer properties. Also, we find that riming has detectable impacts on multifrequency radar observations of the melting layer.

In nature, atmospheric ice particles are usually characterized by a large variety of habits. However, our interpretation of the melting of ice particles is usually based on the assumption of a single class of ice, namely the shapes of ice particles are assumed to be the same. In **Paper III**, we report that two populations of ice particles may produce different radar polarimetric signatures in the melting layer, even though there is still a single radar bright band. The melting signal of small ice needles is utilized to evaluate current melting layer identification methods. The results show that the radar-determined melting layer properties depend on the used radar variable and frequency.

The melting of snowflakes may also have negative effects. When a radar wave penetrates into the melting layer, the signal attenuation can be significant at milimeter wavelengths. Owing to this unknown melting layer attenuation, retrievals made above the melting layer can be highly uncertain for cloud radars. **Paper IV** is the first

observation-based study addressing the melting layer attenuation at W-band. The focus is on the identification of regions satisfying the Rayleigh scattering approximation in multifrequency radar Doppler spectra where dual-wavelength spectral ratios can be related to differential attenuation. The derived melting layer attenuation agrees reasonably well with previously presented modelling results, but differences are found at higher rain rates.

To summarize, this thesis addresses the use of dual-polarization and multifrequency radar observations in revealing precipitation microphysics. The coordinated radar setup facilitates the synergetic analysis of radar observations at various frequencies and from different viewing directions. With more such observations obtained in the future, our understanding on the cloud-to-precipitation processes is expected to be further improved.

References

Aydin, K. and Walsh, T. M. (1999). Millimeter wave scattering from spatial and planar bullet rosettes. *IEEE transactions on geoscience and remote sensing*, 37(2):1138–1150.

Barthazy, E., Henrich, W., and Waldvogel, A. (1998). Size distribution of hydrometeors through the melting layer. *Atmospheric research*, 47:193–208.

Battaglia, A., Kummerow, C., Shin, D.-B., and Williams, C. (2003). Constraining microwave brightness temperatures by radar brightband observations. *Journal of Atmospheric and Oceanic Technology*, 20(6):856–871.

Bauer, P., Baptista, J. P., and De Iulis, M. (1999). The effect of the melting layer on the microwave emission of clouds over the ocean. *Journal of the Atmospheric Sciences*, 56(6):852–867.

Bohren, C. F. and Huffman, D. R. (2008). *Absorption and scattering of light by small particles*. John Wiley & Sons.

Bringi, V., Kennedy, P., Huang, G.-J., Kleinkort, C., Thurai, M., and Notaroš, B. (2017). Dual-polarized radar and surface observations of a winter graupel shower with negative z dr column. *Journal of Applied Meteorology and Climatology*, 56(2):455–470.

Bringi, V. N. and Chandrasekar, V. (2001). *Polarimetric Doppler weather radar: principles and applications*. Cambridge university press.

Carlin, J. T. and Ryzhkov, A. V. (2019). Estimation of melting-layer cooling rate from dual-polarization radar: Spectral bin model simulations. *Journal of Applied Meteorology and Climatology*, 58(7):1485–1508.

Dias Neto, J., Kneifel, S., Ori, D., Trömel, S., Handwerker, J., Bohn, B., Hermes, N., Mühlbauer, K., Lenefer, M., and Simmer, C. (2019). The triple-frequency and polarimetric radar experiment for improving process observations of winter precipitation. *Earth System Science Data*, 11(2):845–863.

Doviak, R., Bringi, V., Ryzhkov, A., Zahrai, A., and Zrnić, D. (2000). Considerations for polarimetric upgrades to operational wsr-88d radars. *Journal of Atmospheric and Oceanic Technology*, 17(3):257–278.

Fabry, F., Austin, G., and Tees, D. (1992). The accuracy of rainfall estimates by radar as a function of range. *Quarterly Journal of the Royal Meteorological Society*, 118(505):435–453.

Fabry, F. and Szyrmer, W. (1999). Modeling of the melting layer. part ii: Electromagnetic. *Journal of the atmospheric sciences*, 56(20):3593–3600.

Fabry, F. and Zawadzki, I. (1995). Long-term radar observations of the melting layer of precipitation and their interpretation. *Journal of the Atmospheric Sciences*, 52(7):838–851.

Field, P. and Heymsfield, A. (2015). Importance of snow to global precipitation. *Geophysical Research Letters*, 42(21):9512–9520.

Field, P. R., Lawson, R. P., Brown, P. R., Lloyd, G., Westbrook, C., Moisseev, D., Miltenberger, A., Nenes, A., Blyth, A., Choularton, T., et al. (2017). Secondary ice production: Current state of the science and recommendations for the future. *Meteorological Monographs*, 58:7–1.

Fletcher, N. H. et al. (2011). *The physics of rainclouds*. Cambridge University Press.

Garrett, T., Fallgatter, C., Shkurko, K., and Howlett, D. (2012). Fall speed measurement and high-resolution multi-angle photography of hydrometeors in free fall. *Atmos. Meas. Tech*, 5(11):2625–2633.

Garrett, T. J., Yuter, S. E., Fallgatter, C., Shkurko, K., Rhodes, S. R., and Endries, J. L. (2015). Orientations and aspect ratios of falling snow. *Geophysical Research Letters*, 42(11):4617–4622.

Giangrande, S. E., Toto, T., Bansemer, A., Kumjian, M. R., Mishra, S., and Ryzhkov, A. V. (2016). Insights into riming and aggregation processes as revealed by aircraft, radar, and disdrometer observations for a 27 april 2011 widespread precipitation event. *Journal of Geophysical Research: Atmospheres*, 121(10):5846–5863.

Gilmore, M. S., Straka, J. M., and Rasmussen, E. N. (2004). Precipitation uncertainty due to variations in precipitation particle parameters within a simple microphysics scheme. *Monthly weather review*, 132(11):2610–2627.

Hallett, J. and Mossop, S. (1974). Production of secondary ice particles during the riming process. *Nature*, 249(5452):26.

Hallett, J., Sax, R. I., Lamb, D., and Murty, A. R. (1978). Aircraft measurements of ice in florida cumuli. *Quarterly Journal of the Royal Meteorological Society*, 104(441):631–651.

Harimaya, T. and Sato, M. (1989). Measurement of the riming amount on snowflakes. *Journal of the Faculty of Science, Hokkaido University. Series 7, Geophysics*, 8(4):355–366.

Haynes, J. M., L'Ecuyer, T. S., Stephens, G. L., Miller, S. D., Mitrescu, C., Wood, N. B., and Tanelli, S. (2009). Rainfall retrieval over the ocean with spaceborne w-band radar. *Journal of Geophysical Research: Atmospheres*, 114(D8).

Heymsfield, A. J. (1982). A comparative study of the rates of development of potential graupel and hail embryos in high plains storms. *Journal of the Atmospheric Sciences*, 39(12):2867–2897.

Heymsfield, A. J., Bansemer, A., Poellot, M. R., and Wood, N. (2015). Observations of ice microphysics through the melting layer. *Journal of the Atmospheric Sciences*, 72(8):2902–2928.

Heymsfield, G. M. (1979). Doppler radar study of a warm frontal region. *Journal of the Atmospheric Sciences*, 36(11):2093–2107.

Hobbs, P. V. and Rangno, A. L. (1985). Ice particle concentrations in clouds. *Journal of the atmospheric sciences*, 42(23):2523–2549.

Hogan, R. J., Field, P., Illingworth, A., Cotton, R., and Choularton, T. (2002). Properties of embedded convection in warm-frontal mixed-phase cloud from aircraft and polarimetric radar. *Quarterly Journal of the Royal Meteorological Society: A journal of the atmospheric sciences, applied meteorology and physical oceanography*, 128(580):451–476.

Houze Jr, R. A. and Medina, S. (2005). Turbulence as a mechanism for orographic precipitation enhancement. *Journal of the atmospheric sciences*, 62(10):3599–3623.

Hubbert, J., Bringi, V., Carey, L., and Bolen, S. (1998). Csu-chill polarimetric radar measurements from a severe hail storm in eastern colorado. *Journal of Applied Meteorology*, 37(8):749–775.

Illingworth, A., Hogan, R., O'connor, E., Bouniol, D., Brooks, M., Delanoë, J., Donovan, D., Eastment, J., Gaussiat, N., Goddard, J., et al. (2007). Cloudnet: Continuous evaluation of cloud profiles in seven operational models using ground-based observations. *Bulletin of the American Meteorological Society*, 88(6):883–898.

Jensen, A. A., Harrington, J. Y., Morrison, H., and Milbrandt, J. A. (2017). Predicting ice shape evolution in a bulk microphysics model. *Journal of the Atmospheric Sciences*, 74(6):2081–2104.

Johnson, D. and Hallett, J. (1968). Freezing and shattering of supercooled water drops. *Quarterly Journal of the Royal Meteorological Society*, 94(402):468–482.

Kain, J. S., Goss, S. M., and Baldwin, M. E. (2000). The melting effect as a factor in precipitation-type forecasting. *Weather and forecasting*, 15(6):700–714.

Keppas, S. C., Crosier, J., Choularton, T., and Bower, K. (2017). Ice lollies: An ice particle generated in supercooled conveyor belts. *Geophysical Research Letters*, 44(10):5222–5230.

Kneifel, S., Kollias, P., Battaglia, A., Leinonen, J., Maahn, M., Kalesse, H., and Tridon, F. (2016). First observations of triple-frequency radar doppler spectra in snowfall: Interpretation and applications. *Geophysical Research Letters*, 43(5):2225–2233.

Kneifel, S., Lerber, A., Tiira, J., Moisseev, D., Kollias, P., and Leinonen, J. (2015). Observed relations between snowfall microphysics and triple-frequency radar measurements. *Journal of Geophysical Research: Atmospheres*, 120(12):6034–6055.

Kollias, P., Albrecht, B. A., Lhermitte, R., and Savtchenko, A. (2001). Radar observations of updrafts, downdrafts, and turbulence in fair-weather cumuli. *Journal of the atmospheric sciences*, 58(13):1750–1766.

Korolev, A. (2007). Limitations of the wegener–bergeron–findeisen mechanism in the evolution of mixed-phase clouds. *Journal of the Atmospheric Sciences*, 64(9):3372–3375.

Korolev, A., McFarquhar, G., Field, P. R., Franklin, C., Lawson, P., Wang, Z., Williams, E., Abel, S. J., Axisa, D., Borrmann, S., et al. (2017). Mixed-phase clouds: Progress and challenges. *Meteorological Monographs*, 58:5–1.

Kruger, A. and Krajewski, W. F. (2002). Two-dimensional video disdrometer: A description. *Journal of Atmospheric and Oceanic Technology*, 19(5):602–617.

Kumjian, M. R., Mishra, S., Giangrande, S. E., Toto, T., Ryzhkov, A. V., and Bansemer, A. (2016). Polarimetric radar and aircraft observations of saggy bright bands during mc3e. *Journal of Geophysical Research: Atmospheres*, 121(7):3584–3607.

Lamb, D. and Verlinde, J. (2011). *Physics and chemistry of clouds*. Cambridge University Press.

Leinonen, J., Lebsock, M. D., Tanelli, S., Sy, O. O., Dolan, B., Chase, R. J., Finlon, J. A., von Lerber, A., Moisseev, D., et al. (2018). Retrieval of snowflake microphysical properties from multifrequency radar observations. *Atmospheric Measurement Techniques*.

Leinonen, J. and Szyrmer, W. (2015). Radar signatures of snowflake riming: A modeling study. *Earth and Space Science*, 2(8):346–358.

Leinonen, J. and von Lerber, A. (2018). Snowflake melting simulation using smoothed particle hydrodynamics. *Journal of Geophysical Research: Atmospheres*, 123(3):1811–1825.

Libbrecht, K. G. (2005). The physics of snow crystals. *Reports on progress in physics*, 68(4):855.

Mason, S., Chiu, C., Hogan, R., Moisseev, D., and Kneifel, S. (2018). Retrievals of riming and snow density from vertically pointing doppler radars. *Journal of Geophysical Research: Atmospheres*, 123(24):13–807.

Mason, S. L., Hogan, R. J., Westbrook, C. D., Kneifel, S., Moisseev, D., and von Terzi, L. (2019). The importance of particle size distribution and internal structure for triple-frequency radar retrievals of the morphology of snow. *Atmospheric Measurement Techniques*, 12(9).

Matrosov, S. Y. (1998). A dual-wavelength radar method to measure snowfall rate. *Journal of Applied Meteorology*, 37(11):1510–1521.

Matrosov, S. Y. (2008). Assessment of radar signal attenuation caused by the melting hydrometeor layer. *IEEE Transactions on Geoscience and Remote Sensing*, 46(4):1039–1047.

Matrosov, S. Y., Clark, K. A., and Kingsmill, D. E. (2007). A polarimetric radar approach to identify rain, melting-layer, and snow regions for applying corrections to vertical profiles of reflectivity. *Journal of applied meteorology and climatology*, 46(2):154–166.

Mitchell, D. L., Zhang, R., and Pitter, R. L. (1990). Mass-dimensional relationships for ice particles and the influence of riming on snowfall rates. *Journal of applied meteorology*, 29(2):153–163.

Mitrescu, C., L'Ecuyer, T., Haynes, J., Miller, S., and Turk, J. (2010). Cloudsat precipitation profiling algorithm-model description. *Journal of Applied Meteorology and Climatology*, 49(5):991–1003.

Moisseev, D., von Lerber, A., and Tiira, J. (2017). Quantifying the effect of riming on snowfall using ground-based observations. *Journal of Geophysical Research: Atmospheres*, 122(7):4019–4037.

Moisseev, D. N., Lautaportti, S., Tyynela, J., and Lim, S. (2015). Dual-polarization radar signatures in snowstorms: Role of snowflake aggregation. *Journal of Geophysical Research: Atmospheres*, 120(24):12644–12655.

Moisseev, D. N., Unal, C. M., Russchenberg, H. W., and Ligthart, L. P. (2002). Improved polarimetric calibration for atmospheric radars. *Journal of Atmospheric and Oceanic Technology*, 19(12):1968–1977.

Morrison, H., Curry, J., and Khvorostyanov, V. (2005). A new double-moment microphysics parameterization for application in cloud and climate models. part i: Description. *Journal of the atmospheric sciences*, 62(6):1665–1677.

Morrison, H. and Grabowski, W. W. (2008). A novel approach for representing ice microphysics in models: Description and tests using a kinematic framework. *Journal of the Atmospheric Sciences*, 65(5):1528–1548.

Morrison, H. and Milbrandt, J. A. (2015). Parameterization of cloud microphysics based on the prediction of bulk ice particle properties. part i: Scheme description and idealized tests. *Journal of the Atmospheric Sciences*, 72(1):287–311.

Morrison, H., van Lier-Walqui, M., Fridlind, A. M., Grabowski, W. W., Harrington, J. Y., Hoose, C., Korolev, A., Kumjian, M. R., Milbrandt, J. A., Pawlowska, H., et al.

(2020). Confronting the challenge of modeling cloud and precipitation microphysics. *Journal of Advances in Modeling Earth Systems*, page e2019MS001689.

Mossop, S. (1985). The origin and concentration of ice crystals in clouds. *Bulletin of the American Meteorological Society*, 66(3):264–273.

Mülmenstädt, J., Sourdeval, O., Delanoë, J., and Quaas, J. (2015). Frequency of occurrence of rain from liquid-, mixed-, and ice-phase clouds derived from A-Train satellite retrievals. *Geophysical Research Letters*, 42(15):6502–6509.

Newman, A. J., Kucera, P. A., and Bliven, L. F. (2009). Presenting the snowflake video imager (svi). *Journal of Atmospheric and Oceanic technology*, 26(2):167–179.

Ohtake, T. (1969). Observations of size distributions of hydrometeors through the melting layer. *Journal of the Atmospheric Sciences*, 26(3):545–557.

Oraltay, R. and Hallett, J. (1989). Evaporation and melting of ice crystals: A laboratory study. *Atmospheric research*, 24(1-4):169–189.

Oue, M., Kollias, P., Ryzhkov, A., and Luke, E. P. (2018). Toward exploring the synergy between cloud radar polarimetry and doppler spectral analysis in deep cold precipitating systems in the arctic. *Journal of Geophysical Research: Atmospheres*, 123(5):2797–2815.

Oue, M., Kumjian, M. R., Lu, Y., Verlinde, J., Aydin, K., and Clothiaux, E. E. (2015). Linear depolarization ratios of columnar ice crystals in a deep precipitating system over the arctic observed by zenith-pointing Ka-band Doppler radar. *Journal of Applied Meteorology and Climatology*, 54(5):1060–1068.

Petäjä, T., O'Connor, E. J., Moisseev, D., Sinclair, V. A., Manninen, A. J., Väänänen, R., von Lerber, A., Thornton, J. A., Nicoll, K., Petersen, W., et al. (2016). BAECC: A field campaign to elucidate the impact of biogenic aerosols on clouds and climate. *Bulletin of the American Meteorological Society*, 97(10):1909–1928.

Rangno, A. L. and Hobbs, P. V. (2001). Ice particles in stratiform clouds in the arctic and possible mechanisms for the production of high ice concentrations. *Journal of Geophysical Research: Atmospheres*, 106(D14):15065–15075.

Rauber, R. M. and Nesbitt, S. L. (2018). *Radar Meteorology: A First Course*. John Wiley & Sons.

Russchenberg, H. and Ligthart, L. P. (1996). Backscattering by and propagation through the melting layer of precipitation: A new polarimetric model. *IEEE transactions on geoscience and remote sensing*, 34(1):3–14.

Skamarock, W., Klemp, J., Dudhia, J., Gill, D., Barker, D., Duda, M., Huang, X., Wang, W., and Powers, J. (2008). A description of the advanced research wrf version 3, tech. *Note, NCAR/TN*, 475.

Spek, A. L. J., Unal, C. M. H., Moisseev, D. N., Russchenberg, H. W. J., Chandrasekar, V., and Dufournet, Y. (2008). A new technique to categorize and retrieve the microphysical properties of ice particles above the melting layer using radar dual-polarization spectral analysis. *Journal of Atmospheric and Oceanic Technology*, 25(3):482–497.

Stewart, R. E., Marwitz, J. D., Pace, J. C., and Carbone, R. E. (1984). Characteristics through the melting layer of stratiform clouds. *Journal of the Atmospheric Sciences*, 41(22):3227–3237.

Straka, J. M., Zrnić, D. S., and Ryzhkov, A. V. (2000). Bulk hydrometeor classification and quantification using polarimetric radar data: Synthesis of relations. *Journal of Applied Meteorology*, 39(8):1341–1372.

Szeto, K. K., Lin, C. A., and Stewart, R. E. (1988). Mesoscale circulations forced by melting snow. part i: Basic simulations and dynamics. *Journal of the Atmospheric Sciences*, 45(11):1629–1641.

Thompson, G., Rasmussen, R. M., and Manning, K. (2004). Explicit forecasts of winter precipitation using an improved bulk microphysics scheme. part i: Description and sensitivity analysis. *Monthly Weather Review*, 132(2):519–542.

Tiira, J., Moisseev, D. N., von Lerber, A., Ori, D., Tokay, A., Bliven, L. F., and Petersen, W. (2016). Ensemble mean density and its connection to other microphysical properties of falling snow as observed in southern finland. *Atmospheric Measurement Techniques*, 9(9):4825.

Tridon, F., Battaglia, A., and Kollias, P. (2013). Disentangling mie and attenuation effects in rain using a ka-w dual-wavelength doppler spectral ratio technique. *Geophysical Research Letters*, 40(20):5548–5552.

Tyynelä, J., Leinonen, J., Moisseev, D., and Nousiainen, T. (2011). Radar backscattering from snowflakes: Comparison of fractal, aggregate, and soft spheroid models. *Journal of Atmospheric and Oceanic Technology*, 28(11):1365–1372.

Tyynelä, J. and von Lerber, A. (2019). Validation of microphysical snow models using in situ, multifrequency, and dual-polarization radar measurements in finland. *Journal of Geophysical Research: Atmospheres*, 124(23):13273–13290.

Vardiman, L. (1978). The generation of secondary ice particles in clouds by crystal–crystal collision. *Journal of the Atmospheric Sciences*, 35(11):2168–2180.

Verlinde, J., Rambukkange, M. P., Clothiaux, E. E., McFarquhar, G. M., and Eloranta, E. W. (2013). Arctic multilayered, mixed-phase cloud processes revealed in millimeter-wave cloud radar Doppler spectra. *Journal of Geophysical Research: Atmospheres*, 118(23):13–199.

Vogel, J. M. and Fabry, F. (2018). Contrasting polarimetric observations of stratiform riming and nonriming events. *Journal of Applied Meteorology and Climatology*, 57(2):457–476.

von Lerber, A., Moisseev, D., Bliven, L. F., Petersen, W., Harri, A.-M., and Chandrasekar, V. (2017). Microphysical properties of snow and their link to z e–s relations during baecc 2014. *Journal of Applied Meteorology and Climatology*, 56(6):1561–1582.

von Lerber, A., Moisseev, D., Leinonen, J., Koistinen, J., and Hallikainen, M. T. (2014). Modeling radar attenuation by a low melting layer with optimized model parameters at c-band. *IEEE Transactions on Geoscience and Remote Sensing*, 53(2):724–737.

Xie, X., Evaristo, R., Simmer, C., Handwerker, J., and Trömel, S. (2016). Precipitation and microphysical processes observed by three polarimetric x-band radars and ground-based instrumentation during hope. *Atmospheric Chemistry and Physics*, 16(11):7105–7116.

Yokoyama, T., Tanaka, H., Akaeda, K., Ohtani, T., Yoshizawa, N., Yamanaka, M. D., Mita, A., Ishizaka, Y., and Ono, A. (1985). Observation on microphysical processes in the stratiform precipitations including melting layers at mt. fuji. *Journal of the Meteorological Society of Japan. Ser. II*, 63(1):100–111.

Zawadzki, I., Fabry, F., and Szyrmer, W. (2001). Observations of supercooled water and secondary ice generation by a vertically pointing x-band doppler radar. *Atmospheric Research*, 59:343–359.

Zawadzki, I., Szyrmer, W., Bell, C., and Fabry, F. (2005). Modeling of the melting layer. part iii: The density effect. *Journal of the Atmospheric Sciences*, 62(10):3705–3723.